Electronic Supplementary Material (ESI) for New Journal of Chemistry.

Supplementary Information

Porous Carbons Embedded with Nitrogen-Coordinated Cobalt as Exceptional Electrochemical Catalyst for High-Performance Zn-Air Batteries

Shice Wei,‡[a] Fan Zhang,‡[a] Zhenying Chen,[a] Junjie Ding,[b] Bai Xue,*[a] Chenbao Lu,*[a]

[a] School of Chemistry and Chemical Engineering, Shanghai Jiao Tong University, 800 Dongchuan Road, Shanghai 200240, China.

[b] Key Lab for Advanced Materials, Institute of Applied Chemistry, East China University of Science and Technology, 130 Meilong Road, Shanghai 200237, China.

‡ These authors contributed equally to this work.

Address correspondence to E-mail: bxue79@sjtu.edu.cn; castle@sjtu.edu.cn

Materials characterization

The morphology and elemental mapping information of the samples were characterized by scanning electron microscopy (SEM, Sirion 200, 25 kV) and transmission electron microscopy (TEM, JEOL JEM-2010, 200 kV). FT-IR spectroscopy was performed on a Spectrum 100 (Perkin Elmer, Inc., USA) spectrometer with a scan range of 3000-500 cm^{-1}. X-ray diffraction (XRD) measurements were carried out on a RigakuD/Max 2500 X-ray diffractometer with Cu Kα radiation (k=1.54 Å) at age neater voltage of 40 kV and a generator current of 50 mA with a scanning speed of 6 ° min^{-1} over the range 5-80 (2θ). Raman spectra were recorded on a SENTERRA with excitation from the 532 nm line of an Ar-ion laser with a power of about 5 mW. TGA was performed using a Q5000IR (TA Instruments, USA) thermogravimetric analyzer at a heating rate of 20 °C min^{-1} under nitrogen flow. The physic sorption isotherms were measured via an Auto-sorb-iQA3200-4 sorption analyzer (Quantatech Co., USA) based on N_2 adsorption/desorption at 77 K. X-ray photoemission spectroscopy (XPS) measurements were performed on a PHI–5000C ESCA system with Al Kα radiation as an X-ray source for radiation and the C 1s value was set at 284.6 eV for charge corrections.

Electrochemical measurements

The working electrode was prepared by loading a catalyst sample film onto a glassy carbon electrode with a diameter of 5.61 mm. To prepare the ink sample, 5 mg sample was dispersed in 500 μL of a mixture of Nafion (5 wt%, 50 μL) and ethanol (450 μL). After stirring for a day and the sonication for 30 minutes, the homogeneous ink (10 μL) was carefully put on the glass carbon disk electrode and the ink slowly dried in air forming the catalyst sample film. For comparison, the commercial catalyst Pt/C (20%) was prepared under the same method. The potential in this study was correlated to RHE by adding 0.944 V, based on the calibration measurement in H_2-saturated 0.1 M KOH.

The electrochemical measurements using CV, rotating disk electrode (ORR polarization curves, RDE) and RRDE investigations were performed by using a basic bipotentiostat (MSR Rotator from Pine Research Instrumentation, USA) with a three-electrode cell system in which a rotating glassy carbon disk and platinum ring electrode loading samples (Pine Research Instrumentation, USA) as the working electrode, while Pt wire and Ag/AgCl (KCl, 4 M) were counter electrode and reference

electrode, respectively. The electrochemical experiments were carried out in O_2-saturated 0.1 M KOH electrolyte for the ORR. For CV measurements, the potential range was cyclically scanned between –1.0 and 0.1 V (vs Ag/AgCl) at a sweep rate of 100 mV s^{-1} at room temperature after purging O_2 or N_2 gas for 30 minutes. For RDE measurements, the potential range was scanned between –1.0 and 0.1 V (vs Ag/AgCl) at a sweep rate of 10 mV s^{-1} at room temperature after purging O_2 gas for 30 minutes. RDE measurements were performed at different rotating speeds, from 225 to 2500 rpm.

The transferred electron number (n) per oxygen molecule in the ORR process at the electrode can be calculated by the K-L equations (S1)-(S3):

$$\frac{1}{J} = \frac{1}{J_L} + \frac{1}{J_K} = \frac{1}{B\omega^{1/2}} + \frac{1}{J_K} \quad \text{(S1)}$$

$$B = 0.62nFC_0(D_0)^{2/3}\nu^{-1/6} \quad \text{(S2)}$$

$$J_K = nFkC_0 \quad \text{(S3)}$$

where J is the measured current density; J_L and J_K are the diffusion-limiting and kinetic current densities; ω is the angular velocity of the rotating electrode (ω = 2πN, N is the linear rotation speed); F is the Faraday constant (F=96485 C mol^{-1}); C_0 is the concentration of O_2; D_0 is the diffusion coefficient of O_2; ν is the kinematic viscosity of the electrolyte, and k is the electron transfer rate constant. In the electrolyte of O_2-saturated 0.1 M KOH, C_0, D_0, and ν are 1.2×10^{-3} M, 1.9×10^{-5} cm^2 s^{-1}, and 0.01 cm^2 s^{-1}, respectively. For RRDE measurements, the potential range of the disk electrode was scanned between –1.0 and 0.1 V (vs Ag/AgCl) at a sweep rate of 10 mV s^{-1} at room temperature under a rotation rate of 1600 rpm. The ring electrode was held at a constant potential of 0.5 V. The HO_2^- yield (%) and electron transfer number (n) can be calculated by equations (S4) and (S5):

$$HO_2^-\ (\%) = \frac{200 \times \frac{I_R}{N}}{I_D + \frac{I_R}{N}} \quad \text{(S4)}$$

$$n = \frac{4I_D}{I_D + \frac{I_R}{N}} \quad \text{(S5)}$$

where I_D is the disk current and I_R is the ring current. N is the ring collection efficiency, which was provided as 0.37 by manufacture.

The primary Zn-air batteries were tested in laboratory-constructed electrochemical cells. A two-electrode configuration was used by pairing catalytic materials loaded onto a carbon paper electrode (with the catalyst loading of 1.0 mg cm^{-2}) with a Zn foil in the electrolyte of 6 M KOH. A polished Zn plate and a catalyst-coated carbon paper HCP-120) were used as the anode and cathode, respectively. The rechargeable Zn-air batteries were also constructed with the same process of the primary Zn-air batteries, except for using 6 M KOH with 0.1 M $ZnCl_2$ as the electrolyte. Based on the battery design, the area of the gas diffusion layer exposed to the electrolyte was 3.14 cm^2. The preparation of the catalyst ink is the same as that in the measurements of ORR. The catalyst ink was dropped to the gas diffusion layer and then the gas diffusion electrode was dried at 80 °C for 1 h. Single-cell testing of the catalyst was performed using a multichannel potentiostat and a laboratory-constructed Zn-air battery

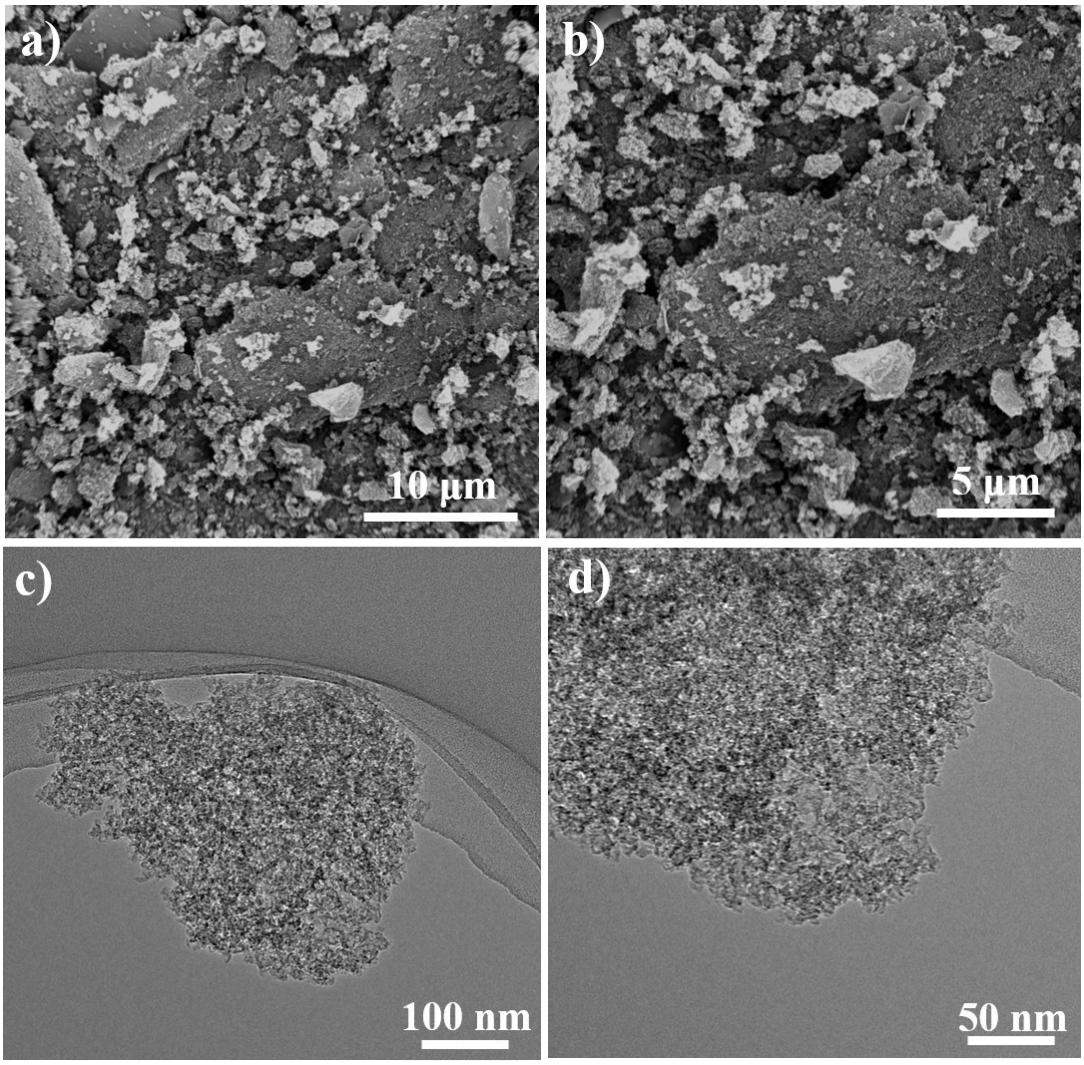

Figure S1 a) and b) SEM images of Co-CTF; c) and d) TEM images of Co-CTF. Co-CTF displays block morphology consisting of plenty of nanoparticles.

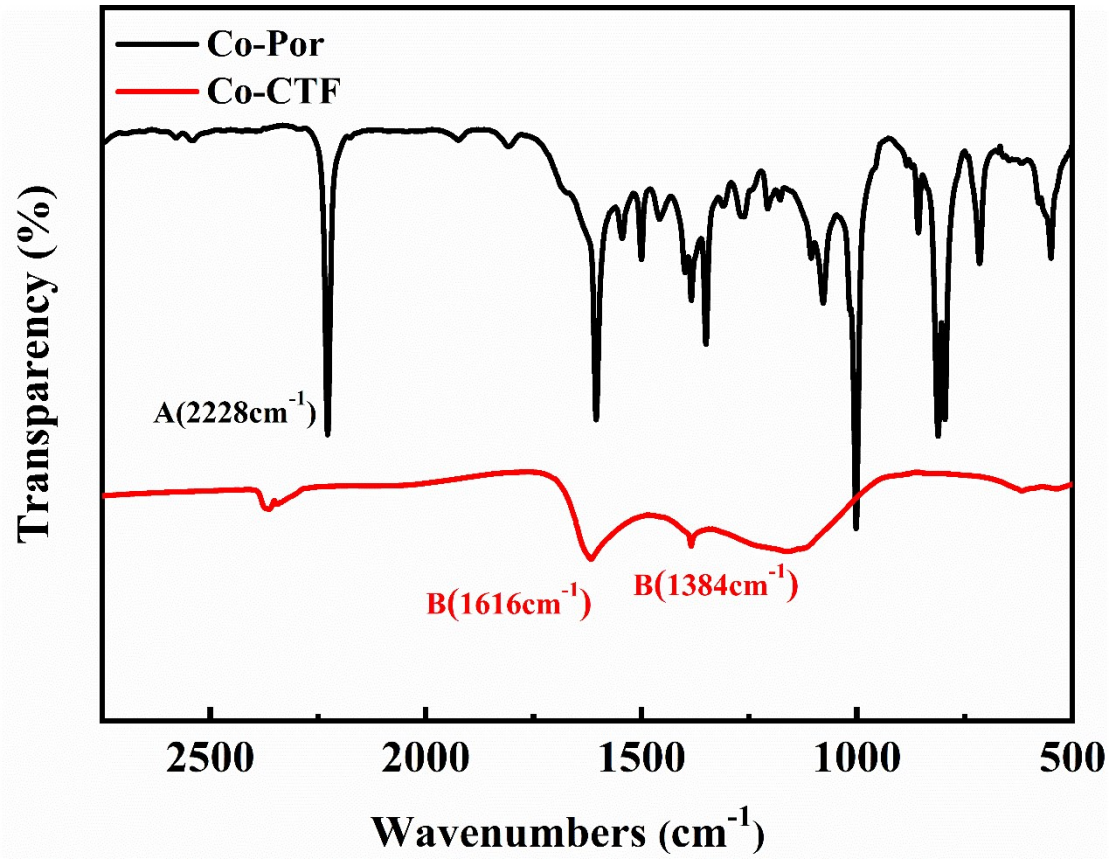

Figure S2 FT-IR spectra of Co-Por and Co-CTF. The disappearance of the cyano band at 2228 cm^{-1} and appearance peaks at 1616 and 1384 cm^{-1} indicate the successful trimerization reaction.

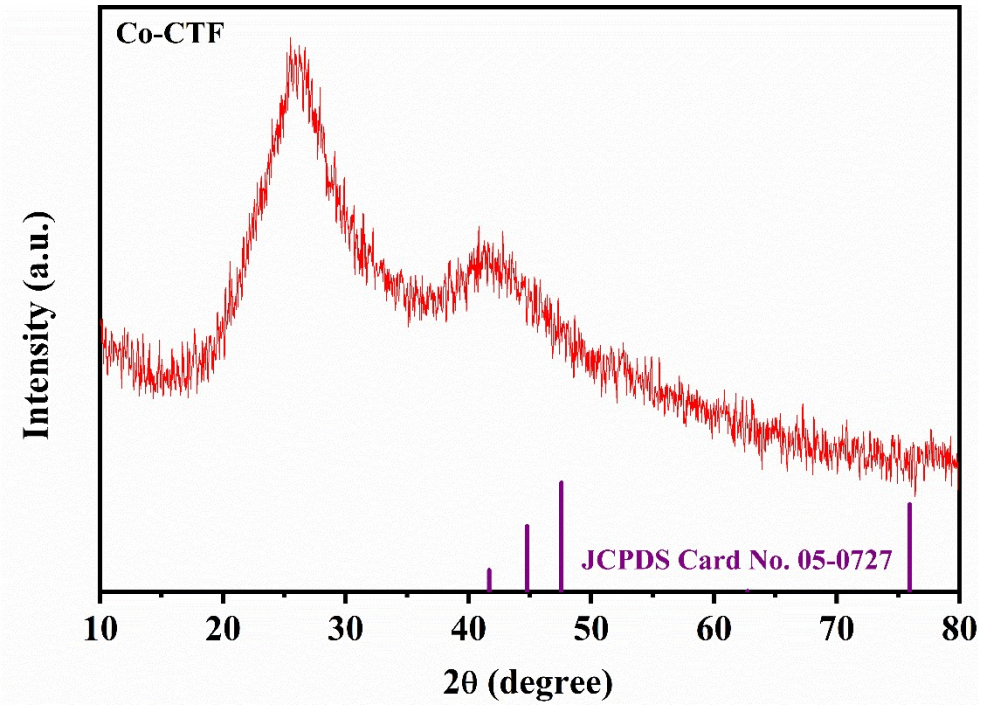

Figure S3 XRD patterns of Co-CTF. Drop lines correspond to Co (JCPDS Card No. 05-0727). No feature X-ray diffraction (XRD) peaks of CTF presented in the XRD patterns (Figure S3), which can be attributed to the harsh polymerization condition.

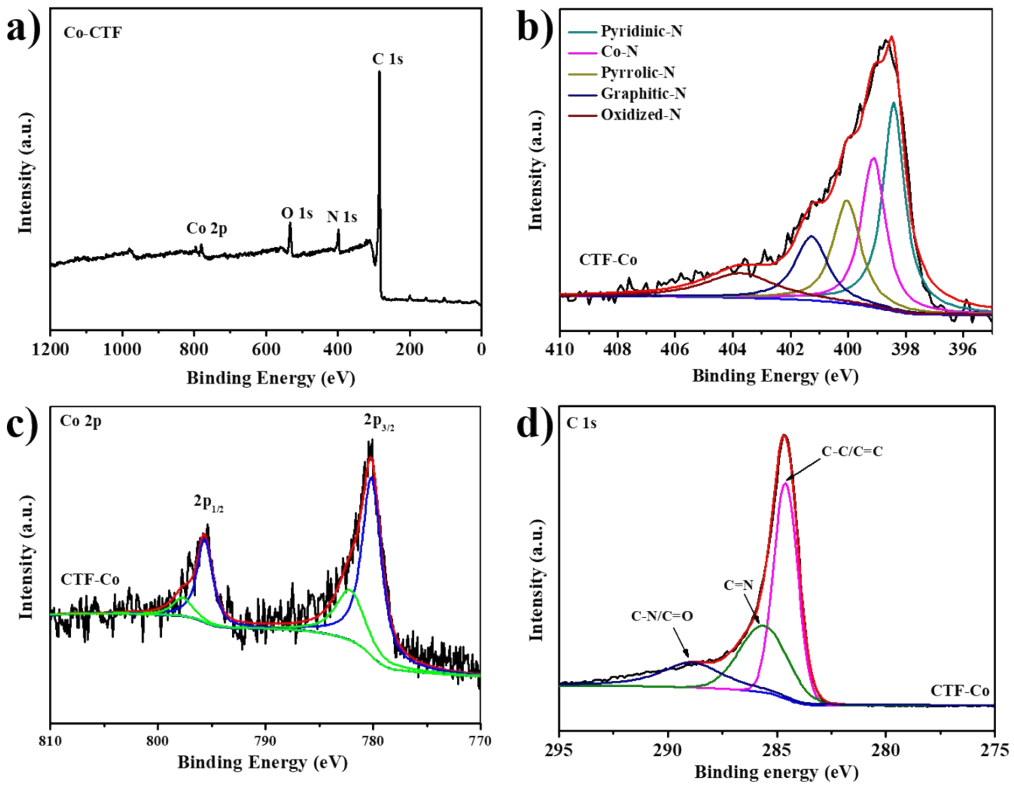

Figure S4 a) XPS spectrum of Co-CTF, indicates the existence of C, N, O and Co elements. b) High-resolution XPS N 1s spectrum of Co-CTF. The nitrogen species can be divided into five individual peaks, corresponding to Pyridinic-N at 398.5 eV, Co-N at 399.3 eV, Pyrrolic-N at 400.8eV, Graphitic-N at 401.7 and Oxidized-N at 403.5, respectively. c) High-resolution XPS Co 2p spectrum of Co-CTF. The Co 2p spectrum can be deconvoluted into the peak at 780.0 and 795.2 eV corresponding to Co 2p3/2 and Co 2p1/2 and the green lines can be attributed to the satellite peak. d) High-resolution XPS C 1s spectrum of Co-CTF. The C 1s spectrum can be deconvoluted into the peak at 284.6, 285.6 and 288.9 corresponding to C-C/C=C, C=N, and C-N/C=O.

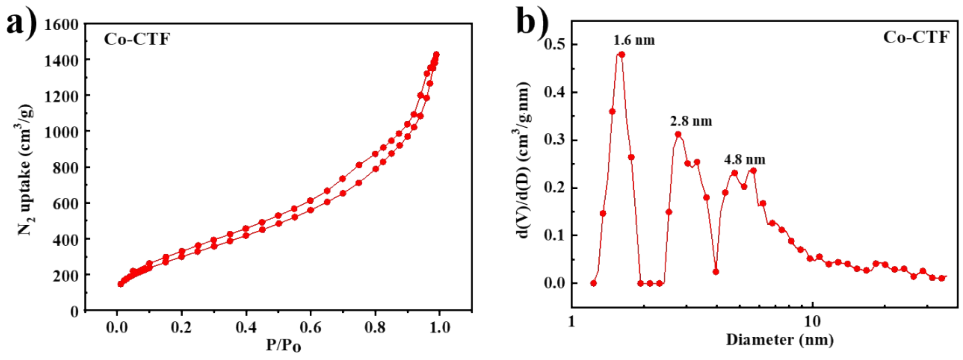

Figure S5 a) N_2-adsorption/desorption isotherm of Co-CTF; b) Corresponding pore-size distribution curves o calculated from the adsorption branch of the isotherms by the DFT method.

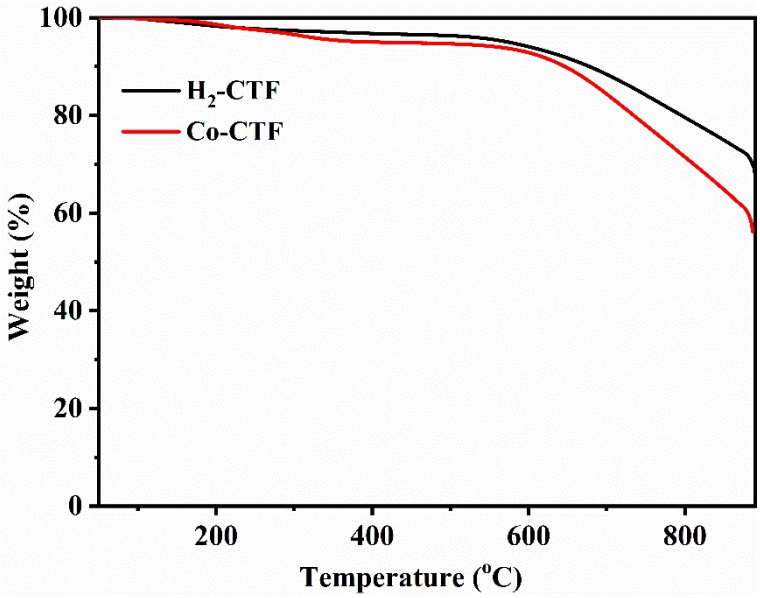

Figure S6 TGA curves of as-prepared H_2-CTF and Co-CTF from 50 to 900 °C under N_2 gas flow with a temperature ramp of 20 °C min^{-1}. Both H_2-CTF and Co-CTF exhibit excellent thermal stability.

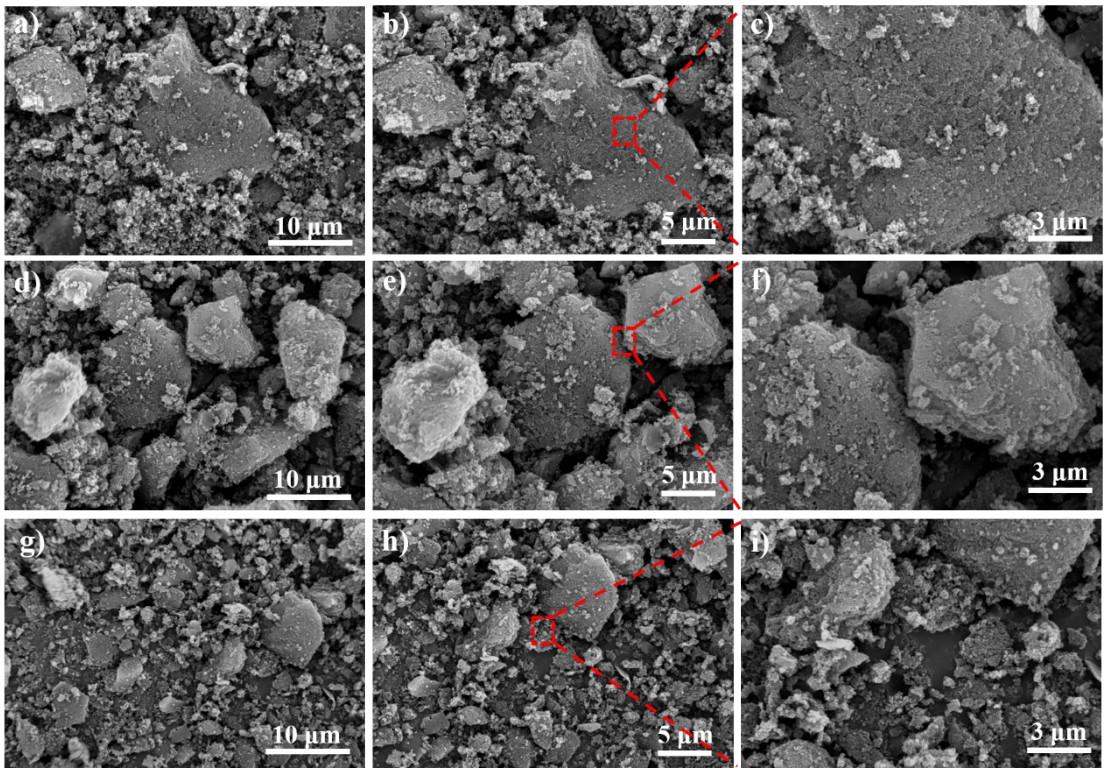

Figure S7 a), b) and c) SEM images of Co/N-PC-800; d), e) and f) SEM images of Co/N-PC-900; g), h) and i) SEM images of Co/N-PC-1000.

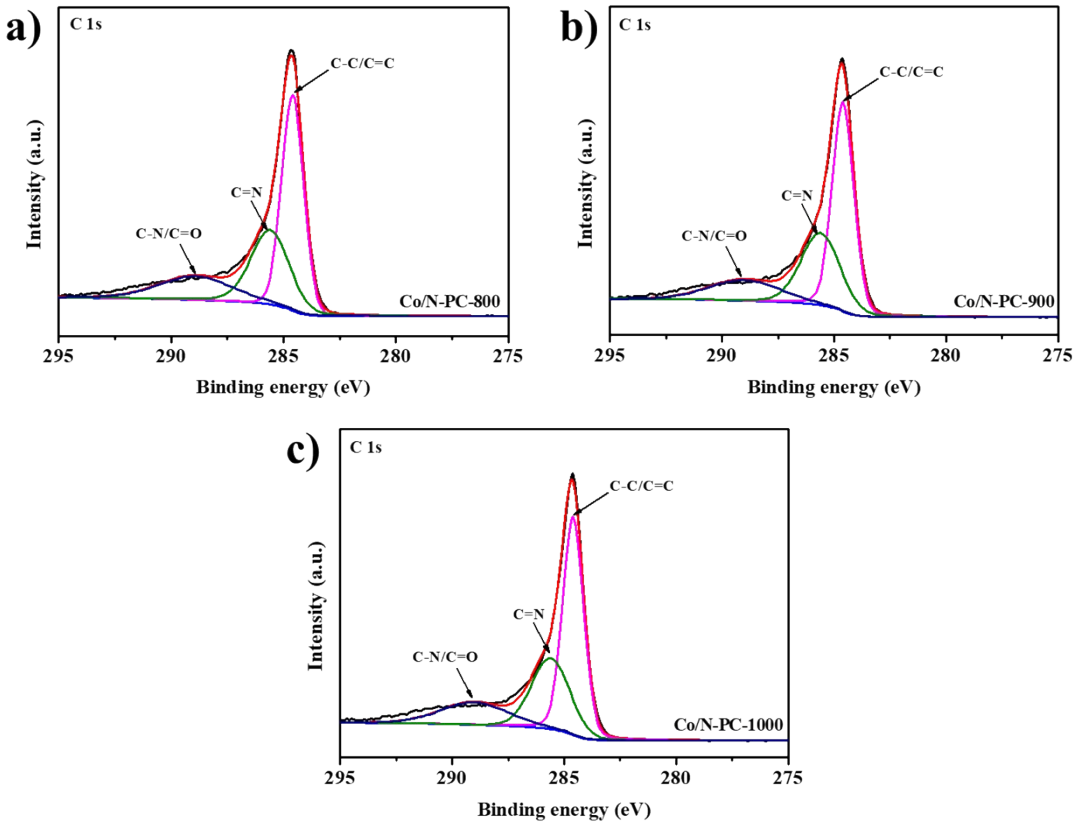

Figure S8 High-resolution C 1s spectra of a) Co/N-PC-800; b) Co/N-PC-900; c) Co/N-PC-1000. The high-resolution XPS C 1s spectra can be deconvoluted into the peaks at 284.6, 285.6 and 288.9 eV corresponding to C-C/C=C, C=N, and C-N/C=O, respectively.

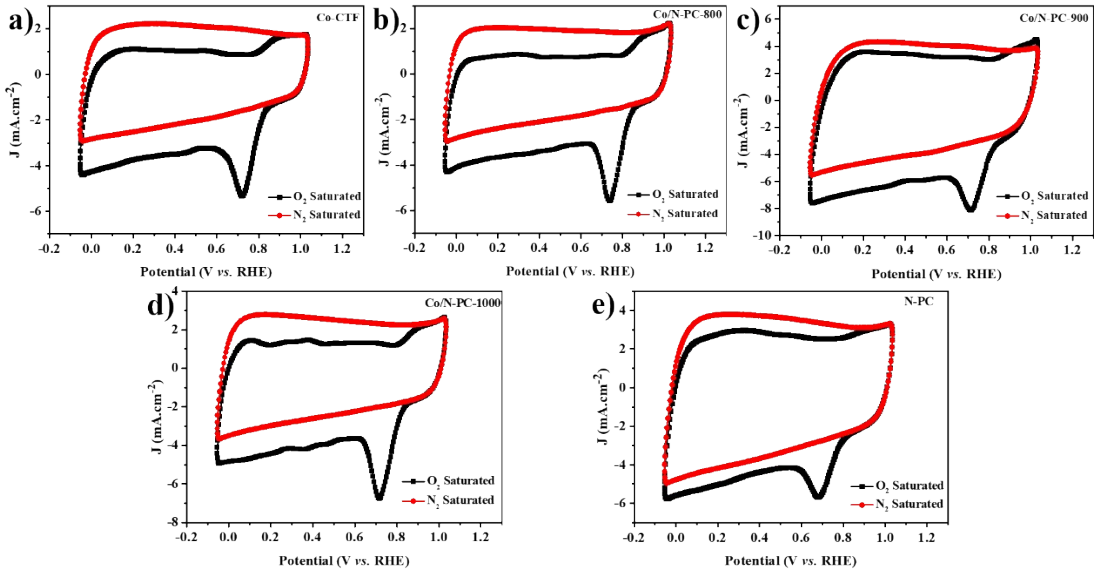

Figure S9 Cyclic voltammetry (CV) curves performed in N_2-saturated (red curves) and O_2-saturated (black curves) 0.1 M KOH of a) Co-CTF; b) Co/N-PC-800; c) Co/N-PC-900; d) Co/N-PC-1000; e) N-PC. A pronounced oxygen reduction current peak at about 0.70 V is observed for all of the prepared materials in O_2-saturated KOH electrolyte, indicating that the materials have the electrocatalytic ability for oxygen reduction reaction.

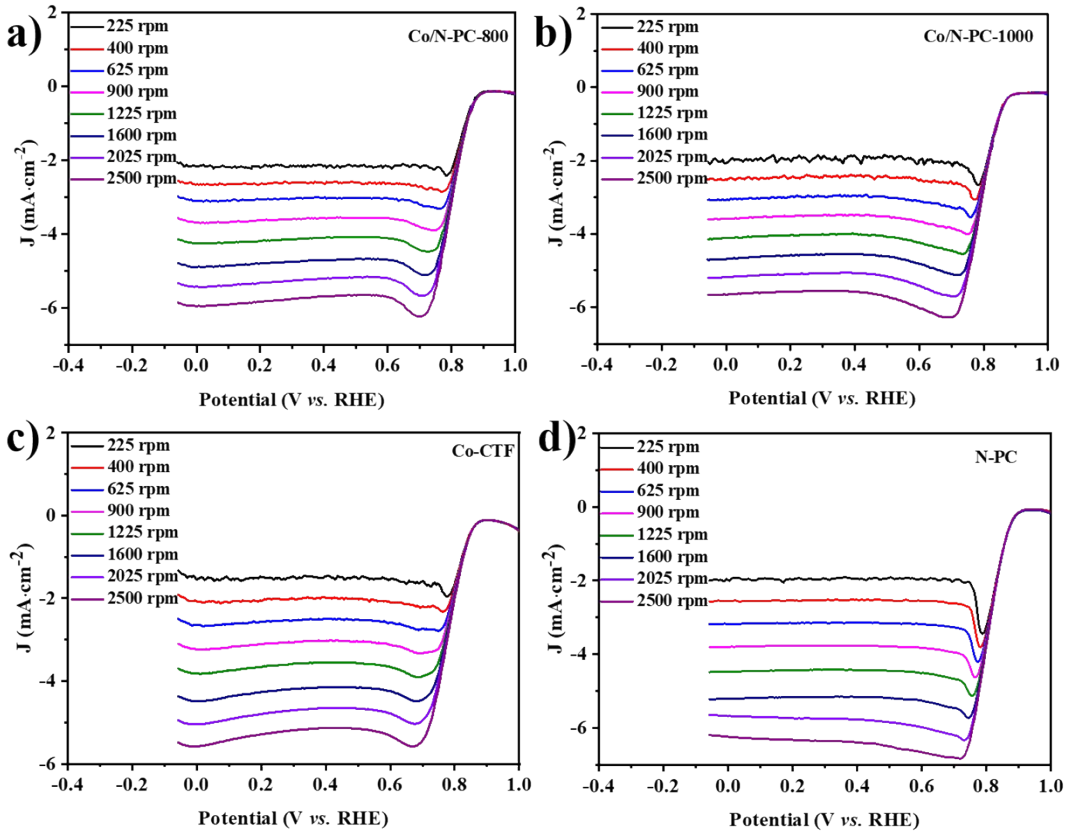

Figure S10 ORR polarization curves of a) Co/N-PC-800; b) Co/N-PC-1000; c) Co-CTF; d) N-PC at different rotation rates from 225 to 2500 rpm.

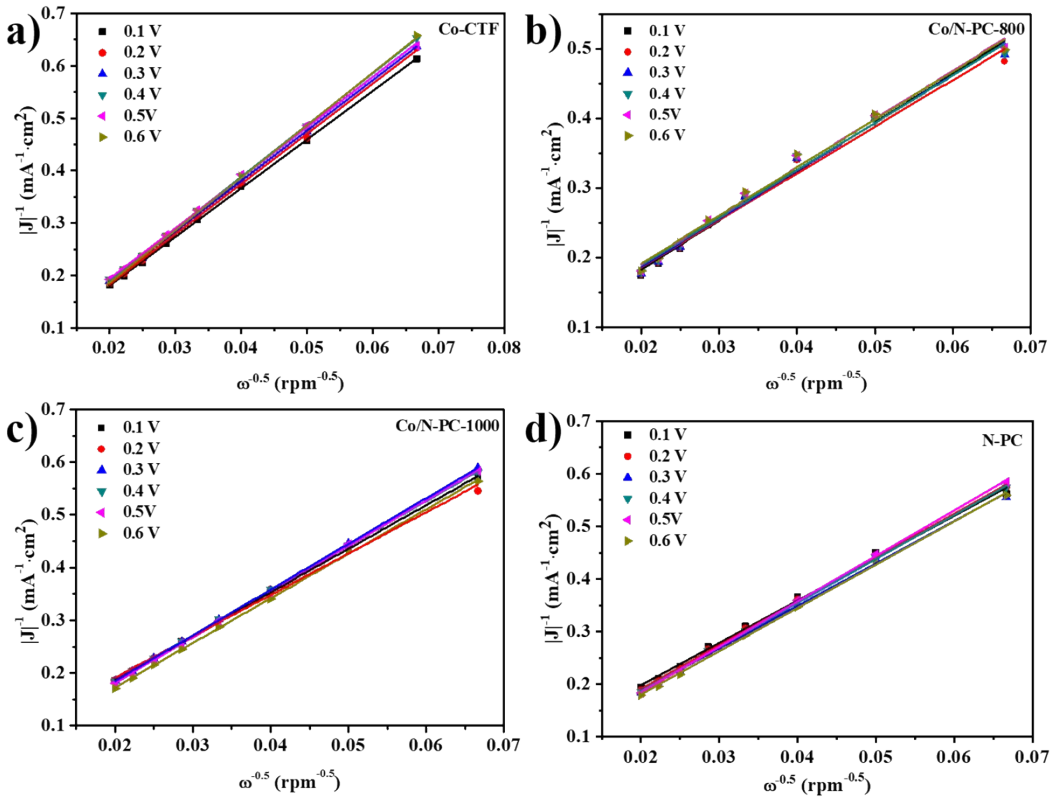

Figure S11 Koutecky–Levich plots of a) Co-CTF; b) Co/N-PC-800; c) Co/N-PC-1000; d) N-PC obtained from ORR polarization curves at different electrode potentials. All of these K-L plots at different potentials exhibit a good linear relationship, indicating the first-order reaction kinetics to the dissolved O_2.

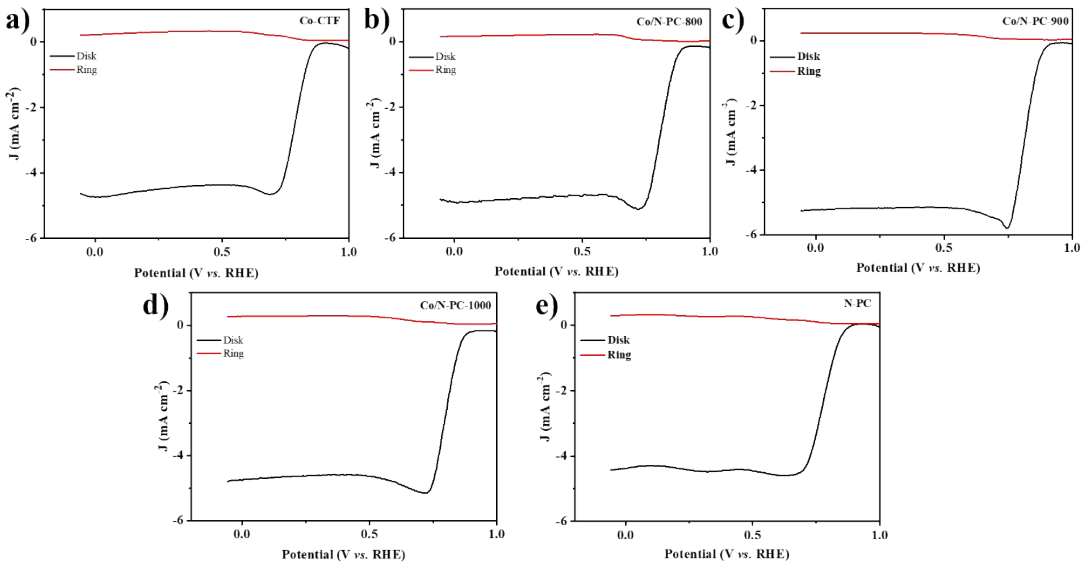

Figure S12 RRDE curves of a) Co-CTF; b) Co/N-PC-800; c) Co/N-PC-900; d) Co/N-PC-1000; e) N-PC in O_2-saturated 0.1 M KOH solution. All samples were measured at a rotation rate of 1600 rpm.

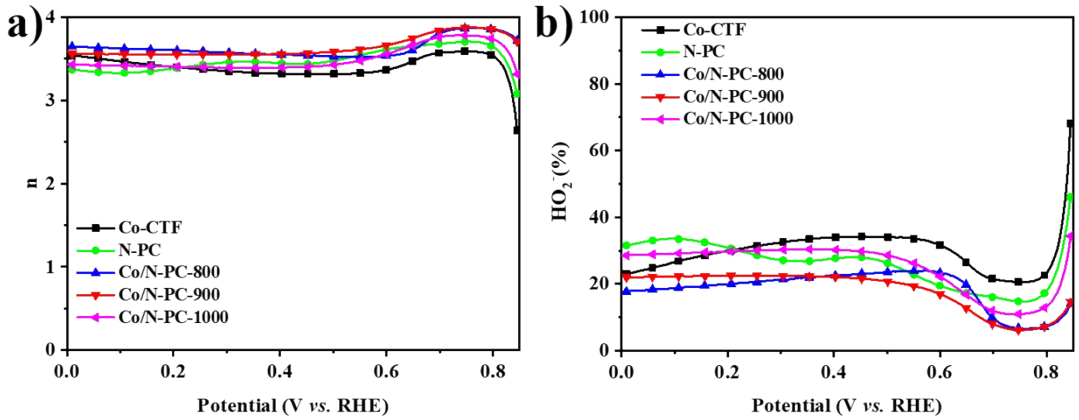

Figure S13 a) Electron transfer number (n) of Co-CTF, N-PC, Co/N-PC-800, Co/N-PC-900 and Co/N-PC-1000; b) HO_2^- yield of Co-CTF, N-PC, Co/N-PC-800, Co/N-PC-900 and Co/N-PC-1000.

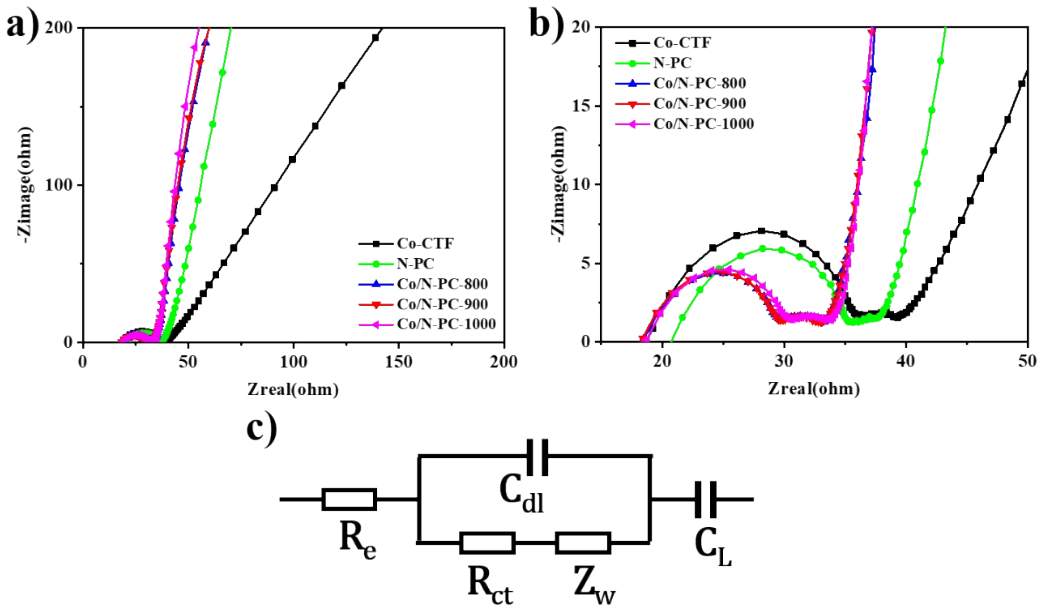

Figure S14 a) and b) Nyquist plots of Co-CTF, N-PC, Co/N-PC-800, Co/N-PC-900 and Co/N-PC-1000; c) The electrical equivalent circuit used for fitting impedance spectra. R_e is the electrolyte resistance, C_{dl} and R_{ct} are the double-layer capacitance and charge-transfer resistance, respectively, Z_w is the Warburg impedance, and C_L is the limit capacitance. The calculated R_{ct} is 15.9 for Co-CTF, 14.8 for N-PC, 10.8 for Co/N-PC-800, 10.9 for Co/N-PC-900 and 11.2 for Co/N-PC-1000, respectively.

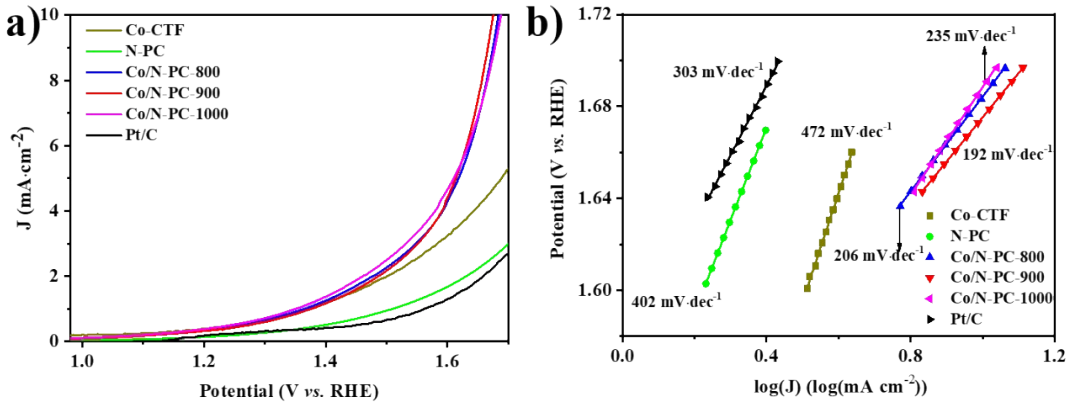

Figure S15 a) OER polarization curves of Co-CTF, N-PC, Co/N-PC-800, Co/N-PC-900, Co/N-PC-1000 and commercial Pt/C in O_2-saturated 0.1 M KOH a sweep rate of 10 mV·s^{-1} at a rotation rate of 1600 rpm; b) Tafel plots of Co-CTF, N-PC, Co/N-PC-800, Co/N-PC-900, Co/N-PC-1000 and commercial Pt/C.

Table S1. N_2 sorption data for obtained materials.

Sample	S_{BET}/ (m^2 g^{-1}) [a]	$S_{langmuir}$/ (m^2 g^{-1}) [b]	V_{Tot}/ (cm^3 g^{-1}) [c]	D_{av}/ (nm) [d]
Co-CTF	1151	1787	2.21	7.67
Co/N-PC-800	911	1530	1.94	8.65
Co/N-PC-900	987	1484	1.68	6.80
Co/N-PC-1000	874	1436	1.49	6.81

[a] Surface area (m^2 g^{-1}) calculated from the nitrogen adsorption based on the BET model.

[b] Surface area (m^2 g^{-1}) calculated from the nitrogen adsorption isotherms based on the Langmuir model.

[c] The total pore volume (cm^3 g^{-1}) calculated at $P/P_0 = 0.99$.

[d] Average pore diameter.

Table S2. The elemental contents of N, Co, O, C and the percentage of different nitrogen species in Co-CTF, N-PC, Co/N-PC-800, Co/N-PC-900 and Co/N-PC-1000 based on XPS results.

Sample	N wt.%						Co	O	C
	Total	Pyridinic-N	Co-N	Pyrrolic-N	Graphitic-N	Oxidized-N	wt.%	wt.%	wt.%
Co-CTF	6.57	32	24	19	14	11	2.63	7.25	83.54
N-PC	2.18	29	0	32	20	19	0	7.14	90.69
Co/N-PC-800	2.9	19	20	24	16	21	1.77	7.74	87.59
Co/N-PC-900	2.12	13	17	27	26	17	1.24	6.23	90.40
Co/N-PC-1000	1.63	12	14	29	25	20	0.77	4.50	93.10

Table S3 The ORR performance of prepared materials and Pt/C from linear sweep voltammograms (LSVs) polarization curves.

Catalysts	Onset potential (V vs RHE)	Half-wave potential (V vs RHE)	J_L[a] (mA cm^{-2})	J_k[b] (mA cm^{-2})
Co-CTF	0.87	0.79	4.74	3.23
N-PC	0.87	0.78	4.37	2.35
Co/N-PC-800	0.89	0.81	4.92	7.56
Co/N-PC-900	0.91	0.83	5.23	13.25
Co/N-PC-1000	0.90	0.81	4.74	3.90
Pt/C	0.95	0.81	5.65	7.99

[a] Limiting current density.

[b] Kinetic current density at 0.8 V.c

Table S4 Comparison of the onset and half-wave potentials for ORR of non-noble metal catalysts systems from literature reprints and this work in alkaline medium.

Catalysts	Electrolyte	Onset potential (V vs RHE)	Half-wave potential (V vs RHE)	J_L [a] (mA cm^{-2})	Ref.
CoP-CMP800	0.1 M KOH	0.88	0.82	4.62	[1]
GNC-Co	0.1 M KOH	0.88	0.75	4.50	[2]
Co@NCNT-700	0.1 M KOH	0.89	0.80	4.75	[3]
Fe-N/C-800	0.1 M KOH	0.93	0.81	4.77	[4]
Co/N-C-800	0.1 M KOH	0.83	0.77	5.26	[5]
Co@Co3O4/NC-2	0.1 M KOH	0.89	0.74	4.50	[6]
CoN/C	0.1 M KOH	0.85	0.81	4.58	[7]
Cu-CTF/CP	0.1 M NaOH	0.91	0.79	5.25	[8]
FeNC-800	0.1 M KOH	0.89	0.815	5.21	[9]
Fe3C/C-700	0.1 M KOH	0.94	0.83	4.20	[10]
NiO/CoN PINWs	0.1 M KOH	0.89	0.68	4.42	[11]
D-Co@CNG	0.1 M KOH	0.88	0.81	4.66	[12]
Co-N_x-C graphene	0.1 M KOH	0.84	0.80	4.75	[13]
NP-Fe-NHPC	0.1 M KOH	0.97	0.88	5.50	[14]
MnO/Co/PGC	0.1 M KOH	0.95	0.78	6.00	[15]
NC@Co-NGC DSNCs	0.1 M KOH	0.92	0.82	5.25	[16]
Co/N-PC-900	0.1 M KOH	0.91	0.83	5.23	This work

[a] Limiting current density.

Reference:

[1] Z.-S. Wu, L. Chen, J. Liu, K. Parvez, H. Liang, J. Shu, H. Sachdev, R. Graf, X. Feng, K. Müllen, *Adv. Mater.*, 2014, **26**, 1450-1455.

[2] S. Li, D. Wu, C. Cheng, J. Wang, F. Zhang, Y. Su, X. Feng, *Angew. Chem., Int. Ed.*, 2013, **125**, 12327-12331.

[3] Y. Hao, Z. Lu, G. Zhang, Z. Chang, L. Luo, X. Sun, *Energy Technol.*, 2016, **5**, 1265-1271.

[4] W. Niu, L. Li, X. Liu, N. Wang, J. Liu, W. Zhou, Z. Tang, S. Chen, *J. Am. Chem. Soc.*, 2015, **137**, 5555-5562.

[5] Y. Su, Y. Zhu, H. Jiang, J. Shen, X. Yang, W. Zou, J. Chen, C. Li, *Nanoscale*, 2014, **6**, 15080-15089.

[6] A. Aijaz, J. Masa, C. Rösler, W. Xia, P. Weide, A. J. R. Botz, R. A. Fischer, W. Schuhmann, M. Muhler, *Angew. Chem., Int. Ed.*, 2016, **55**, 4087-4091.

[7] L. An, W. Huang, N. Zhang, X. Chen, D. Xia, *J. Mater. Chem. A*, 2014, **2**, 62-65.

[8] K. Iwase, T. Yoshioka, S. Nakanishi, K. Hashimoto, K. Kamiya, *Angew. Chem., Int. Ed.*, 2015, **54**, 11068-11072.

[9] K. Yuan, S. Sfaelou, M. Qiu, D. Lützenkirchen-Hecht, X. Zhuang, Y. Chen, C. Yuan, X. Feng, U. Scherf, *ACS Energy Lett.*, 2018, **3**, 252-260.

[10] Y. Hu, J. O. Jensen, W. Zhang, L. N. Cleemann, W. Xing, N. J. Bjerrum, Q. Li, *Angew. Chem., Int. Ed.*, 2014, **53**, 3675-3679.

[11] J. Yin, Y. Li, F. Lv, Q. Fan, Y.-Q. Zhao, Q. Zhang, W. Wang, F. Cheng, P. Xi, S. Guo, *ACS Nano*, 2017, **11**, 2275-2283.

[12] Y. Huang, Q. Liu, J. Lv, D. D. Babu, W. Wang, M. Wu, D. Yuan, Y. Wang, *J. Mater. Chem. A*, 2017, **5**, 20882-20891.

[13] C. Tang, B. Wang, H.-F. Wang, Q. Zhang, *Adv. Mater.*, 2017, **29**, 1703185.

[14] G. Chen, P. Liu, Z. Liao, F. Sun, Y. He, H. Zhong, T. Zhang, E. Zschech, M. Chen, G. Wu, J. Zhang, X. Feng, *Adv. Mater.*, 2020, **32**, 1907399.

[15] X. F. Lu, Y. Chen, S. Wang, S. Gao, X. W. Lou, *Adv. Mater.*, 2019, **31**, 1902339.

[16] S. Liu, Z. Wang, S. Zhou, F. Yu, M. Yu, C.-Y. Chiang, W. Zhou, J. Zhao, J. Qiu, *Adv. Mater.*, 2017, **29**, 1700874.